Int. J. Electrochem. Sci., 14 **(2019)** 4917 – 4932, doi: 10.20964/2019.06.51

International Journal of
ELECTROCHEMICAL
SCIENCE
www.electrochemsci.org

Influence of Zn(II) and Sodium Dodecyl Benzene Sulfonate as Electrolyte Additives on the Electrochemical Performance of Mg-10Li-3Al-3Zn Electrodes in a NaCl solution

Jinhao Su, Xinyue Zhao, Guangyu Li, Lili Zhang[*]*, Guixiang Wang*[*]*, Aidong Liu*

College of Materials Science and Chemical Engineering, Harbin Engineering University, Harbin, 150001, People's Republic of China
[*]E-mail: zhanglili1984@hrbeu.edu.cn, wangguixiang@hrbeu.edu.cn

Received: 7 February 2019 / *Accepted:* 5 April 2019 / *Published:* 10 May 2019

The influence of electrolyte additives on the electrochemical performance of Mg-10Li-3Al-3Zn electrodes was studied. After mixing various concentrations of Zn^{2+} and sodium dodecyl benzene sulfonate (SDBS) in a 0.7 M NaCl electrolyte solution, magnesium alloy electrodes discharged at 25 °C. Potentiodynamic polarization, potentiostatic oxidation, electrochemical impendence spectroscopy (EIS), scanning electron microscopy (SEM) and energy dispersive spectrometry (EDS) were utilized to analyze the electrochemical performance of the electrode. The combination of Zn^{2+} and SDBS improved the corrosion resistance of the electrode. Mg-10Li-3Al-3Zn electrodes retained the highest discharge current density and the smallest polarization resistance in the electrolyte solution including 2.0 mM Zn^{2+} and 1.0 mM SDBS at three various constant potentials: –1.4, –1.2 and –1.0 V. The additives accelerated the breaking and shedding of oxides on the electrode surface to expand the effective discharge area. The combination of 2.0 mM Zn^{2+} and 1.0 mM SDBS had the optimal effect on improving the electrochemical performance of Mg-10Li-3Al-3Zn electrodes.

Keywords: Mg-10Li-3Al-3Zn electrodes; electrochemical performance; electrolyte additives; Zn^{2+}; sodium dodecyl benzene sulfonate

1. INTRODUCTION

The Mg-H_2O_2 semi-fuel cell is a new kind of power source that is desirable for autonomous underwater vehicles [1-3] for the following reasons. Compared to Mg/air batteries [4-7], magnesium primary batteries and magnesium ion secondary batteries [8-12], Mg-H_2O_2 semi-fuel cells have a higher theoretical voltage reaching 4.14 V [13]. They also have the advantages of high energy density, stable discharge voltage, simple structure, long storage life, short charging time and environmental acceptability [14,15].

The typical Mg-H_2O_2 semi-fuel cell utilizes magnesium alloys as anodes and carbon fiber supported Pd-Ir as cathodes: the anode and cathode electrolytes are separated by proton exchange membrane (Nafion-115) of seawater and seawater-H_2SO_4-H_2O_2, respectively. During discharging, magnesium alloys are oxidized and hydrogen peroxide is reduced. The electrode reactions, cell reaction and standard potentials for this semi-fuel cell system are as follows [16]:

Anode reaction: $Mg \rightarrow Mg^{2+} + 2e^-$, $E^0 = 2.37$ V vs. SHE (1)

Cathode reaction: $H_2O_2 + 2H^+ + 2e^- \rightarrow 2H_2O$, $E^0 = 1.77$ V vs. SHE (2)

Cell reaction: $Mg + H_2O_2 + 2H^+ \rightarrow Mg^{2+} + 2H_2O$, $E^0_{cell} = 4.14$ V (3)

Because of its high chemical activity, magnesium reacts easily with water, which generates a large amount of hydrogen. Meanwhile, the self-corrosion of hydrogen evolution (4) occurs, which results in reducing anode efficiency [17].

$$Mg + 2H_2O \rightarrow Mg(OH)_2 + H_2 \quad (4)$$

$Mg(OH)_2$ forms a passive film on the electrode surface to prevent contact between the electrolyte and electrodes. The reduction in the effective contact area decreases the discharge current density and increases anodic overpotential. Meanwhile, the passive film also hinders the migration of magnesium ions and the reaction between magnesium metal and the electrolyte to increase polarization resistance [17]. When the cell begins to discharge, the slow electrode response results in a hysteresis effect. In addition, during discharging, because the surface passive film gradually splits gradually with the positive shift of the polarization potential, more magnesium is exposed to produce the self-corrosion hydrogen evolution reaction, which results in a "negative difference effect [18]" and decreases the discharge efficiency of magnesium alloy electrodes.

There are two methods to resolve the above problems and enhance the integral electrochemical performances of the magnesium alloy anode. One is doping other metal elements in magnesium alloys. “Corrosion inhibition” elements such as aluminum, zinc and manganese can constitute microprimary cells with magnesium alloys [7,19,20]. Due to their high hydrogen overpotential, the added metal elements can slow the anodic oxidation of magnesium alloys to decrease the hydrogen evolution corrosion rate. “Activation” elements such as gallium, lithium, mercury and cerium can destroy the formation of dense passive films in order to decrease the ionic conduction resistance on the passive film surface [20-22]. A second method is adding additives to the electrolyte solution. At present, additives are mainly divided into two categories: inorganic salts such as gallate, chromate and stannate [23] and organic salts such as sulfocarbamide, aromatic carboxylate and trizinc methyl ammonium hydrochloride [24]. These two methods can both inhibit self-evolution hydrogen corrosion and passivation of magnesium electrodes in the process of discharge to play the roles of "corrosion inhibitors" and "activators".

Adding lithium can raise the discharge activity of magnesium alloys, can weaken the hysteresis effect and can increase the specific energy of alloy electrodes. Furthermore, magnesium-lithium-based alloys have been applied in the fields of aerospace, the electron industry and automobiles due to the merits of excellent formability, high electrical, high thermal conductivities, high Faradic capacity, negative standard electrode potentials and ultralight mass [7,25-27]. Wang et al. [28] investigated the discharge and corrosion behaviors of Mg-3 wt.% Al alloys with different contents of lithium in a 3.5 wt.% NaCl aqueous solution. They found that doping Mg-3 wt.% Al with 8 wt.% lithium negatively shifted

the discharge potentials and inhibited self-discharge, therefore leading to a low corrosion current density, negative discharge potentials, and high anodic efficiencies of the metal anode. Sivashanmugam et al. [29] found that a Mg-Li/$MgCl_2$/CuO battery with Mg-13Li as the anode material had higher working voltage and capacity than that with Mg-Al alloy as the anode, with a maximum anode current efficiency of 81%. Many researchers have conducted detailed studies of adding alloy elements to Mg-Li-based alloy electrodes to enhance their discharge performances. Wang et al. [30] studied the discharge and corrosion behaviors of Mg-Li-Al-Ce-Y-Zn alloy in 3.5 wt.% NaCl solution. They found that the addition of zinc decreased the corrosion current density of Mg-Li-Al-Ce-Y-Zn alloys. Moreover, the anodic efficiency of Mg-Li-Al-Ce-Y-Zn alloys at 10 mA cm^{-2} reached (60.6±0.2)%, which is higher than that of AP65 magnesium alloys. Lv et al. [15] found that, compared to Mg-7.5Li-3.5Al electrodes, Mg-7.5Li-3.5Al-1Y electrodes have higher electrochemical activity and utilization efficiency. In addition, Mg-7.5Li-3.5Al-1Y electrodes have no lagging effect or negative difference effect. Rong-Chang Zeng et al. [27] noted that fine grains of calcium could improve the mechanical properties and corrosion resistance of Mg-9.29Li-0.88Ca alloys and change the pitting corrosion mode of magnesium alloys into full-scale corrosion.

At the same time, the effects of electrolyte additives on the discharge performances of cells with Mg-Li-based alloys as electrodes were also studied. Lv et al. [31] found that Na_2SnO_3 significantly enhanced the discharge current density and electrochemical activity of Mg-8Li electrodes. Specifically, at a constant potential of –0.8 V, 0.20 mM Na_2SnO_3 enhanced the current density of Mg-8Li electrodes by approximately 5.0 $mA \cdot m^{-2}$ in a 0.7 mol L^{-1} NaCl electrolyte solution. Cao et al. [32] studied the influence of Ga_2O_3 as an electrolyte additive on the discharge behaviors of Mg-8Li-3Al-1Ce, Mg-8Li-3Al and AZ31 electrodes in a 0.7 M NaCl solution. The results showed that Ga_2O_3 increased the discharge current density of three kinds of electrodes to varying degrees and significantly shortened their transition time. Synchronously, the current efficiencies of three types of alloy electrodes were all improved. Specifically, the current efficiency of Mg-8Li-3Al-1Ce alloys was raised by 6% and reached approximately 87%.

According to the literature, most studies regard single electrolyte additives instead of inorganic salt-organic salt composite additives. In this study, various concentrations of Zn^{2+}-sodium dodecyl benzene sulfonate (SDBS) additives were prepared to investigate the influence of electrolyte additives on the electrochemical behaviors of Mg-10Li-3Al-3Zn electrodes in a 0.7 M NaCl electrolyte solution. This study contributes to electrochemical studies and fills a gap in utilizing inorganic salt-organic salt additives to improve the electrochemical performance of magnesium-lithium-based alloys.

2. EXPERIMENTAL

2.1. Materials and chemicals

Pure magnesium (99.99%), pure lithium (99.99%), pure aluminum (99.99%) and pure zinc (99.99%) were all purchased from Taiyuan Jingcheng Magnesium Alloy Science and Technology Co., Ltd. (Taiyuan, China). Sodium chloride, zinc sulfate and sodium dodecyl benzene sulfonate were all

bought from Tianjin Tianli Chemical Reagent Co., Ltd. (Tianjin, China). Acetone was received from Tianjin Fuyu Fine Chemical Development Center (Tianjin, China) and argon was purchased from Harbin Liming Gas Co., Ltd. (Harbin, China).

Deionized water was utilized in all measurements and all chemicals were of analytical purity.

2.2. Melting of the Mg-Li-based alloy

The experimental alloy was prepared through smelting ingot castings of the purchased high purity metals in a refractory in a vacuum induction smelting furnace (KGPS, Jinkai, Jinzhou, China). After putting magnesium and other alloy components into induction furnace, the furnace was immediately evacuated to 1.0×10^{-2} Pa and simultaneously charged with ultrahigh purity argon as a protective gas. When the pressure inside the furnace was roughly the same as that of the outside atmosphere, alternating current power connected to the induction furnace was applied to start melting the metal under argon protection with the halt of injecting ultrahigh purity argon. After slow heating for 10 min at a furnace power of 2 kW, the furnace power was increased to 4 kW, and the metal continued to be heated for 30 min until completely mixed and melted. Through a tundish, the molten metals were poured into a stainless steel mold that had been preheated for 3 h at 200 °C inside a drying baker. Under the cover of the protective gas, after cooling for 2 h to ambient temperature, the molten metals became as-cast alloys.

2.3. Analysis of alloy composition

An inductively coupled plasma emission spectrometer (ICP) (IRIS Intrepid II, Thermoelectric, USA) was utilized to analyze the compositions of the prepared alloy. The compositions of various metal elements in the prepared alloy are listed in Table 1.

Table 1. Chemical compositions of the alloy (wt.%).

Alloys	Mg	Li	Al	Zn
Mg-10Li-3Al-3Zn	84	10	3	3

2.4. Preparation of alloy electrode

The Mg-10Li-3Al-3Zn alloy was machined to a 20 mm × 20 mm × 2 mm rectangular sheet before it was utilized as the working electrode. Prior to each test, the experimental surface of the electrode must be gradually and continuously polished with 300#, 600#, 800# and 1200# metallographic emery papers and then burnished with an abrasive finishing machine until the experimental surface is smooth and clean. After it was washed with deionized water, the electrode was immersed in acetone for 15 min for degreasing and was then cleaned again with deionized water. Afterward, the electrode immediately was installed into the electrochemical cell.

2.5. Experiments and characterization

The electrochemical measurements were performed in a conventional three-electrode cell consisting of a saturated calomel electrode (SCE) as the reference electrode, a platinum net as the auxiliary electrode, and a magnesium alloy sheet as the working electrode, whose contact area with the electrolyte was 1.00 cm^2. The electrochemical experiments were conducted in a 0.7 M NaCl solution involving various concentrations of Zn^{2+}-SDBS electrolyte additives (0.0 + 0.0, 0.5 + 2.5, 1.0 + 2.0, 1.5 + 1.5, 2.0 + 1.0 and 2.5 + 0.5 mM). Prior to measurements, all oxygen dissolved in the mixed electrolyte was removed through pouring ultrahigh-purity argon on it for 15 min. All measurements were performed under the cover of the protective gas at room temperature.

The electrochemical workstation (CHI760E, Chenhua, Shanghai, China) that was connected to the conventional three-electrode system was used to measure potentiodynamic polarization, potentiostatic oxidation and perform electrochemical impendence spectroscopy (EIS). After adjusting the sweep voltage (−2.20 to −1.15 V) and the scan rate (5 mV s^{-1}), the potentiodynamic polarization curves were obtained to investigate the corrosion potential and corresponding the corrosion current of Mg-10Li-3Al-3Zn electrodes. Potentiostatic current-time curves were tested by separately enabling the magnesium alloy anode discharge for 1000 s at four different constant potentials (−1.4, −1.2, −1.0 and −0.8 V). The EIS measurements were conducted in the frequency range of $0.1-10^5$ Hz with an AC amplitude of 5 mV. After potentiostatic oxidation, a scanning electron microscope (SEM) (S4800, Jeol, Tokyo, Japan) at 500-times magnification and 20 kV working voltage and an energy dispersive spectrometer (EDS) were utilized to observe the surface morphology of the Mg-10Li-3Al-3Zn electrodes.

3. RESULTS AND DISCUSSION

3.1. Potentiodynamic polarization

Figure 1 shows the potentiodynamic polarization curves recorded for Mg-10Li-3Al-3Zn electrodes, which were acquired from a 0.7 M NaCl electrolyte solution that included various concentrations of Zn^{2+}-SDBS electrolyte additives. The corrosion potentials (E_{corr}) and corresponding corrosion current densities (i_{corr}) are summarized in Table 2.

As is shown in Figure 1 and Table 2, overall, various concentrations of additives altered the corrosion potential and corresponding self-corrosion current density of the electrode to varied degrees. The addition of additives improved the corrosion potential indicating that the corrosion resistance of the electrode was strengthened. By improving the concentration of Zn^{2+} and reducing the concentration of SDBS, the corrosion potential exhibited a tendency to first increase and then decrease. Meanwhile, the corresponding corrosion current density displayed a completely opposite trend. When 1.0 mM Zn^{2+} and 2.0 mM SDBS were mixed in the electrolyte, E_{corr} increased from –1.599 V to –1.526 V and i_{corr} decreased from 129.60 $\mu A \cdot m^{-2}$ to 23.68 $\mu A \cdot cm^{-2}$, indicating that the corrosion resistance of the working electrode was greatly enhanced. The reason for this is that, on one hand, due to the replacement reaction between magnesium metal and zinc ions, the addition of Zn^{2+} made more zinc particles with higher

hydrogen evolution overpotential cover the electrode surface to hinder the hydrogen evolution reaction. On the other hand, according to the adsorption principle [33], due to the sorption of superficial active molecules, SDBS in a high concentration constituted multilayer protective films on the electrode surface that inhibited the self-evolution hydrogen corrosion of the magnesium alloys. Eventually, Zn^{2+} and SDBS together inhibited corrosion of the magnesium alloy electrodes. Yanzhou Lv [31] conducted a similar measurement for improving the corrosion resistance of Mg-8Li electrodes through mixing Na_2SnO_3 in NaCl electrolyte. 0.05 mM additive improved E_{corr} from -1.552 V to -1.505 V, which maximized the corrosion resistance of Mg-8Li electrodes in a NaCl solution. In contrast, the variation of i_{corr} was inconsistent with the change in E_{corr}. In addition, the effect of 0.05 mM Na_2SnO_3 on the corrosion resistance was less than 1.0 mM Zn^{2+} and 2.0 mM SDBS because the latter enhanced the E_{corr} of Mg-10Li-3Al-3Zn electrodes in a NaCl electrolyte from –1.599 V to –1.526 V. Polarization curves of Mg-Li-Al-Ce-Y and Mg-Li-Al-Ce-Y-Zn alloys in a 3.5 wt.% NaCl solution were obtained by Naiguang Wang et al. [30]. They found that doping zinc declined i_{corr} of Mg-Li-Al-Ce-Y alloys from 897 $mA \cdot cm^{-2}$ to 197 $mA \cdot cm^{-2}$, whose rate of decline was approximately 78%. By comparison, 1.0 mM Zn^{2+} and 2.0 mM SDBS decreased i_{corr} of Mg-10Li-3Al-3Zn alloys from 129.60 $\mu A \cdot m^{-2}$ to 23.68 $\mu A \cdot cm^{-2}$, whose rate of decline was approximately 82%. Therefore, elemental zinc as an electrolyte additive with the combination of SDBS has a better influence on improving corrosion resistance of Mg-Li-based alloys in a NaCl solution than it as an alloying agent. Yanzhou Lv [34] found that E_{corr} of Mg-8Li-3Al-0.5Zn and Mg-8Li-3Al-1.0Zn electrodes in a 0.7 M NaCl solution were –1.58 V and –1.57 V respectively, which were lower than Mg-Li-based alloy electrodes with similar compositions in a NaCl solution including Zn^{2+} and SDBS. It illustrates that the inorganic salt-organic salt binary additives can strengthen the corrosion resistance of Mg-Li-based alloys.

As the concentration of Zn^{2+} and SDBS respectively continued to increase and decrease, E_{corr} showed a continuous, negative shift to –1.587 V, while i_{corr} gradually increased to 183.80 $\mu A \cdot cm^{-2}$. This can be explained in that the persistent addition of Zn^{2+} made zinc particles cover the magnesium alloy surface completely, such that no extra magnesium in the alloy surface was replaced by redundant zinc ions. In addition, SO_4^{2-} provided an acidic environment and the SDBS at a lower concentration formed a sparse and uneven film on the electrode surface, which both accelerated the self-corrosion rate and weakened the corrosion resistance.

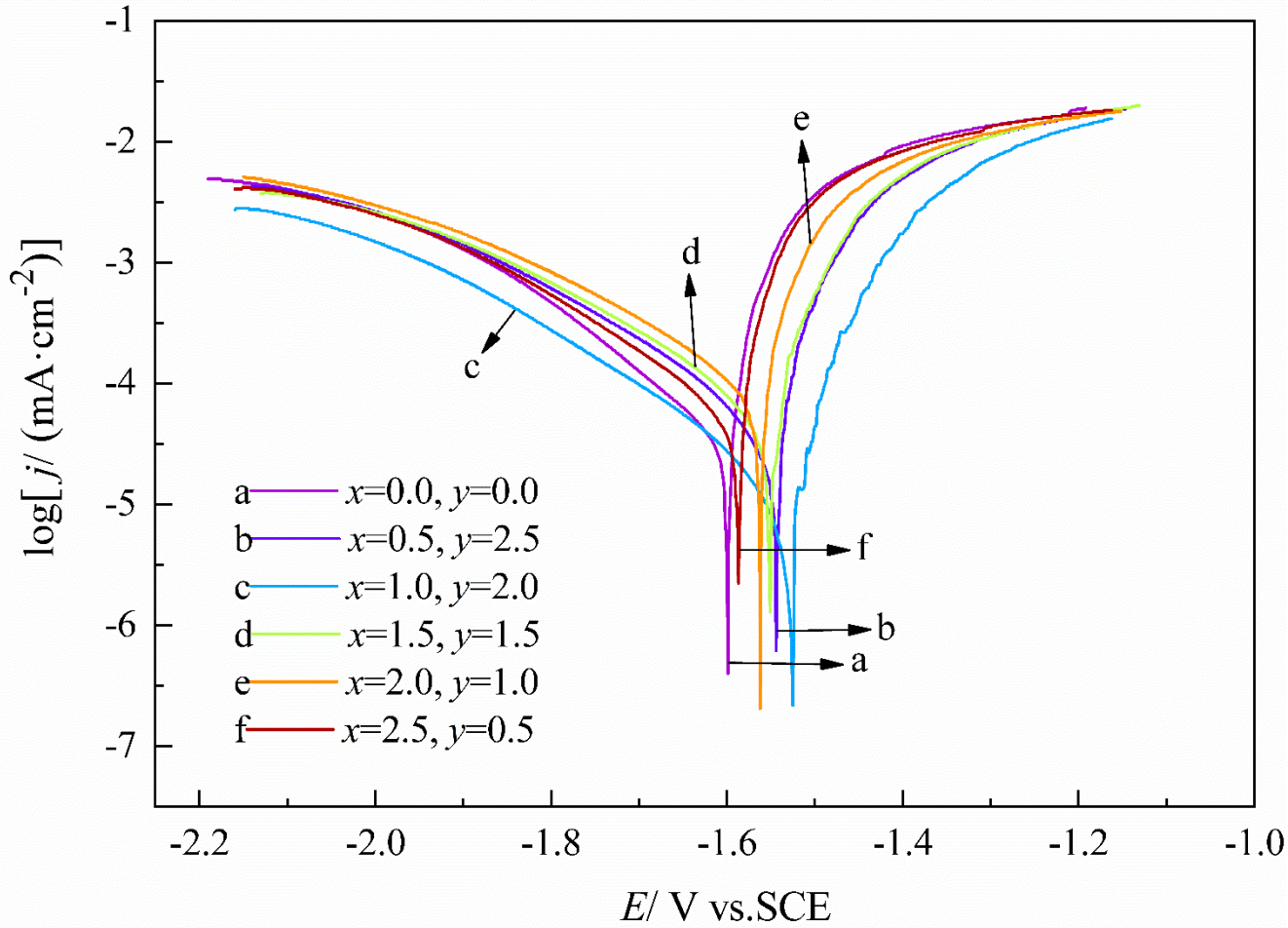

Figure 1. Potentiodynamic polarization curves recorded on Mg-10Li-3Al-3Zn electrodes that were acquired from a 0.7 M NaCl solution including *x* mM Zn^{2+} and *y* mM SDBS.

Table 2. Corrosion potential (E_{corr}) and corrosion current density (i_{corr}) obtained from the potentiodynamic polarization curves recorded in Figure 1.

x mM Zn^{2+} + *y* mM SDBS	E_{corr} (V)	i_{corr} (μA·cm^{-2})
x=0.0, *y*= 0.0	–1.599	129.60
x=0.5, *y*= 2.5	–1.544	80.80
x=1.0, *y*= 2.0	–1.526	23.68
x=1.5, *y*= 1.5	–1.551	81.58
x=2.0, *y*= 1.0	–1.562	238.90
x=2.5, *y*= 0.5	–1.587	183.80

In summary, the electrolyte additives enhanced the corrosion potential of the magnesium alloy anode, indicating that Zn^{2+}-SDBS additives improved the corrosion resistance of Mg-10Li-3Al-3Zn electrodes in the electrolyte solution. The mixture of 1.0 mM Zn^{2+} and 2.0 mM SDBS had the optimal influence on corrosion inhibition of the magnesium alloy electrodes.

3.2. Potentiostatic measurements

Current-time curves of Mg-10Li-3Al-3Zn electrodes measured at four various constant potentials of –1.4, –1.2, –1.0 and –0.8 V in a 0.7 M NaCl electrolyte solution including various concentrations of Zn^{2+} and SDBS are displayed in Figures 2(a), 2(b), 2(c) and 2(d).

As a whole, the various concentrations of electrolyte additives affected the anodic current density of magnesium alloy electrodes to various degrees. In each of the four images, the majority of current-time curves appeared as saw tooth-shaped; in particular, the curve representing the solution without complex additives showed the most obvious periodic oscillation phenomenon. This phenomenon can be explained in that, during discharging, the accumulation of oxidation products attached to the electrode surface insulated the electrode surface, and the electrolyte shrank the effective discharge area of the electrode surface, which reduced the discharge current. After accumulation, the oxides fell off the electrode surface, which enlarged the contact area between the internal magnesium alloys and electrolyte and then increased the discharge current. Ultimately, serrated currents appeared. Figure 2(b) shows that the current-time curve representing 2.0 mM Zn^{2+}+1.0 mM SDBS was relatively smooth at –1.2 V, demonstrating that the formed oxides of the electrode surface were easy to shed. A similar phenomenon appeared in the potentiostatic measurements of Mg-5Li-3Al-1La and Mg-8Li-3Al-1La alloys in a sodium chloride solution [1]. The improvement of lithium content made the current-time curve of Mg-8Li-3Al-1La electrodes recorded in a 0.7 M NaCl solution at -1.2 V smoother than those of Mg-5Li-3Al-1La electrodes, which illustrates that the combination of 2.0 mM $Zn^{2+}$and 1.0 mM SDBS has the same influence as lithium in promoting oxide peeling from the electrode surface and activating the electrodes. The discharge current densities at the four constant potentials grew rapidly at the beginning of discharging and then decreased slightly to a steady state value. By enhancing the constant potential, the transition time was simultaneously shortened, illustrating that the hysteresis effect was weakened.

As is shown in Figures 2(a), 2(b) and 2(c), under –1.4, –1.2 and –1.0 V, the additives consisting of 2.0 mM Zn^{2+} and 1.0 mM SDBS respectively raised the current density of the electrode by 0.2, 0.7 and 0.5 $mA \cdot cm^{-2}$ to maxima compared to those without additives. It can be concluded that redundant SO_4^{2-} activated the electrode to reduce anodic polarization, and a small quantity of SDBS formed an uneven surface film to promote the self-corrosion reaction of the electrode. According to a previous literature, the anodic current density of Mg-8Li-3Al-1.0Zn electrodes in a 0.7 M NaCl solution at –1.0 V was approximately 27 $mA \cdot cm^{-2}$ [34], which was smaller than that of Mg–10Li–3Al–3Zn electrodes in an electrolyte including 2.0 mM Zn^{2+} and 1.0 mM SDBS. It illustrates that the combination of Zn^{2+} and SDBS can enhance the discharge activity of Mg-Li-based electrodes with similar components. By contrast, in Figures 2(a), 2(c) and 2(d), other concentrations of additives caused the working electrode to generate a smaller anodic current density than that without additives at –1.4, –1.0 and –0.8 V. Particularly, the mixture of 1.5 mM Zn^{2+} and 1.5 mM SDBS decreased the discharge current density to a minimum, which was approximately 0.7, 2.1 and 3.4 $mA \cdot cm^{-2}$ lower than those without additives. The reason for this is that displaced zinc and multilayer protective films of SDBS covered the electrode to hinder charge transfer, which weakened discharge activity. A similar phenomenon appeared in the potentiostatic measurements of Mg-8Li-3Al-0.5Zn and Mg-8Li-3Al-1.0Zn alloys in a sodium chloride solution [34]. The addition of elemental zinc decreased the anodic current density of Mg-8Li-3Al-0.5Zn

electrodes from 30 mA·cm^{-2} to 27 mA·cm^{-2}, which illustrates that elemental zinc can weakened discharge activity. However, mixing 2.0 mM Zn^{2+} and 1.0 mM SDBS in a NaCl solution can improve the discharge current density of the Mg-Li-based electrode instead of weakening its anodic current density, which indicates that 1.0 mM SDBS can promote the self-corrosion reaction and activate electrodes.

The additives compounded with 2.0 mM Zn^{2+} and 1.0 mM SDBS had the best influence on enhancing the discharge activity of Mg–10Li–3Al–3Zn electrodes because the electrodes held the highest anodic current density in the mixed electrolyte solution at approximately –1.4, –1.2 and –1.0 V.

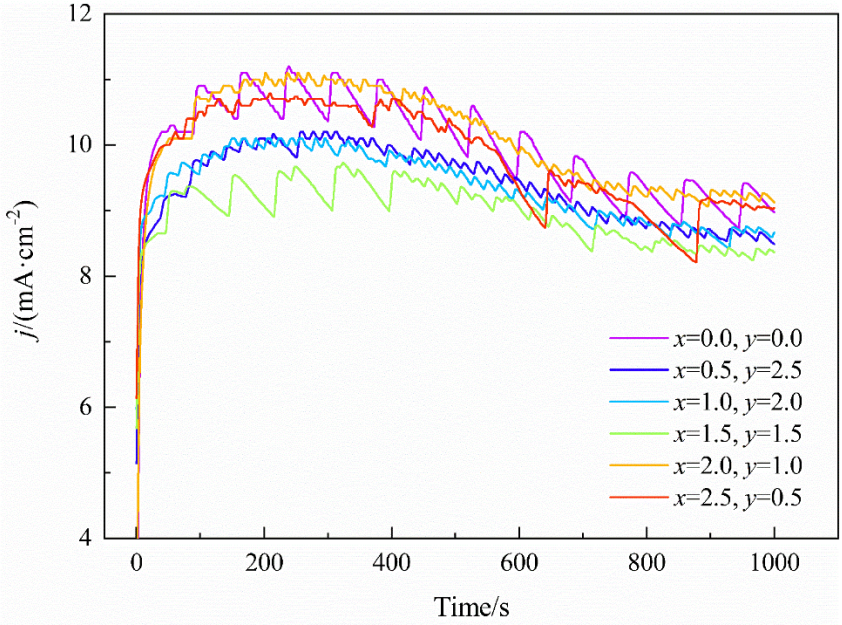

(a)

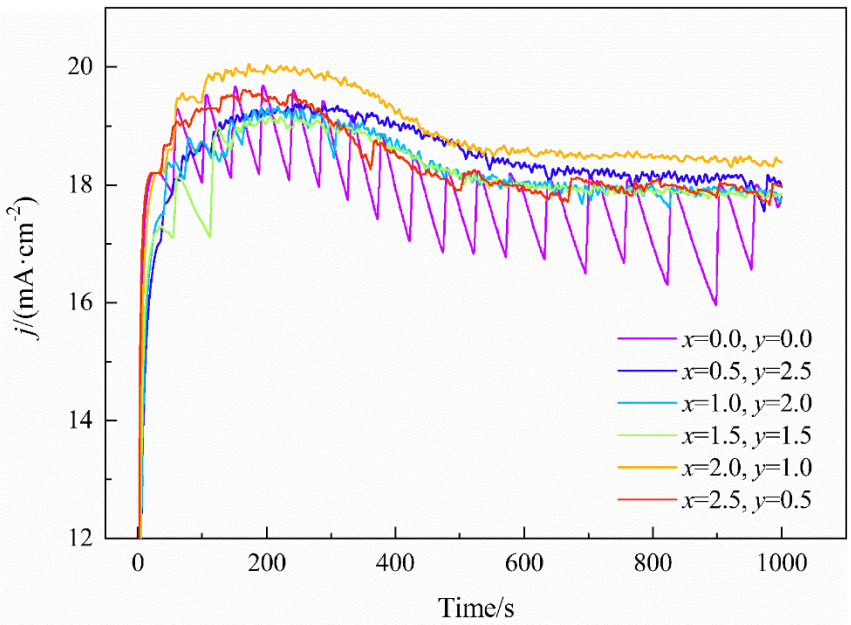

(b)

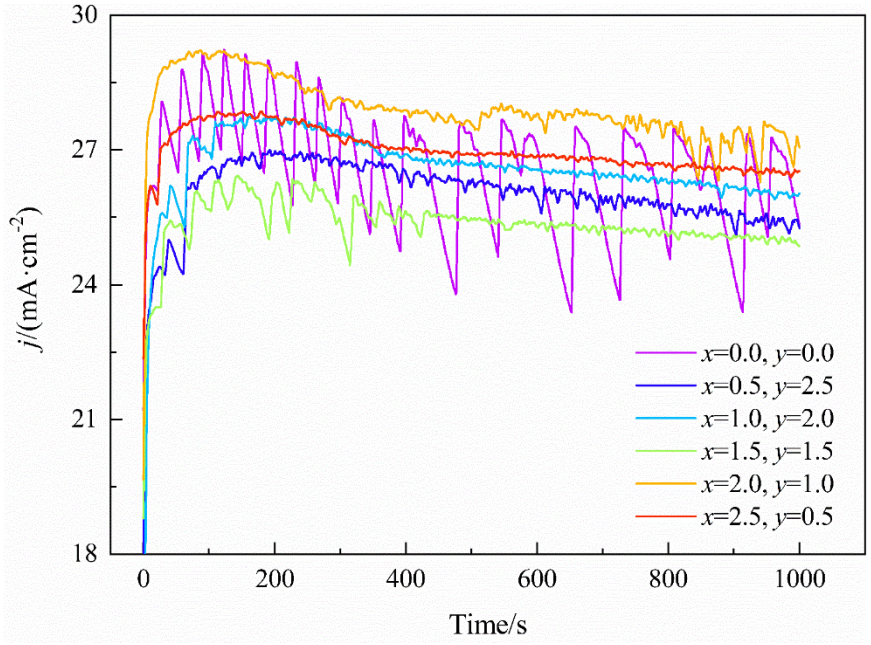

(c)

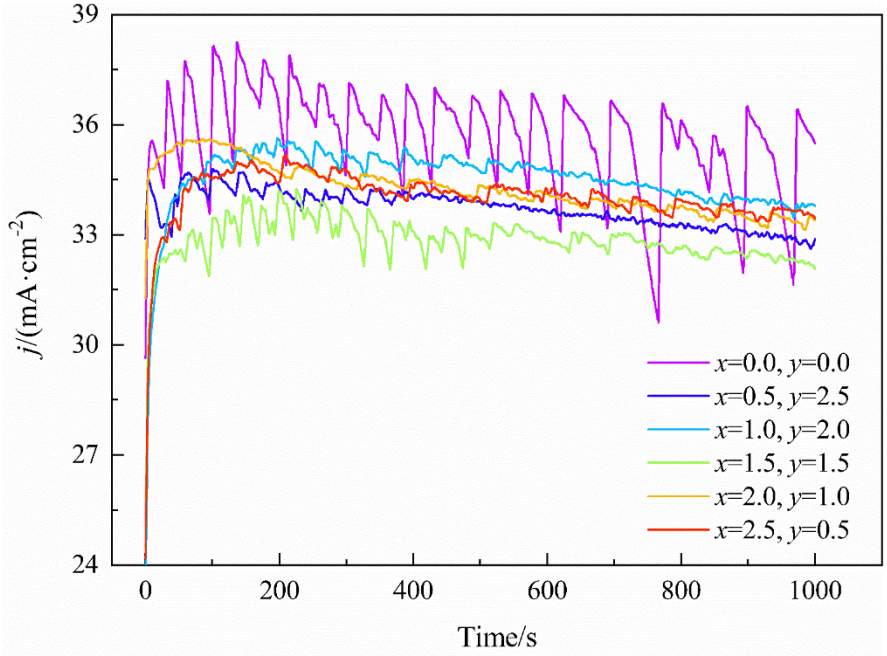

(d)

Figure 2. Current-time curves for Mg-10Li-3Al-3Zn electrodes recorded in a 0.7 M NaCl solution including *x* mM Zn^{2+} and *y* mM SDBS at (a) –1.4 V, (b) –1.2 V, (c) –1.0 V, (d) –0.8 V.

3.3. Electrochemical impedance spectroscopy

Figure 3 exhibits the electrochemical impedance spectroscopies of Mg-10Li-3Al-3Zn electrodes at –1.0 V for 1000 s in a mixed electrolyte solution including various concentrations of Zn^{2+} and SDBS. The selected equivalent circuit diagram is located in the top-left corner of Figure 3. The Nyquist plots exhibit a frequency capacitive loop that results from electric charge transfer, and the diameter of the capacitive loop represents the charge transfer resistance, or in other words, the polarization resistance

(R_p) [35,36]. The EIS electrochemical parameters are summarized in Table 3. Mg-10Li-3Al-3Zn electrodes had an increasing impedance value in the following order with the concentration of Zn^{2+} + SDBS: 2.0 + 1.0 mM< 0.5 + 2.5 mM< 2.5 + 0.5 mM< 0.0 + 0.0 mM< 1.0 + 2.0 mM< 1.5 + 1.5 mM, indicating that R_p changed variably under the action of various concentrations of additives.

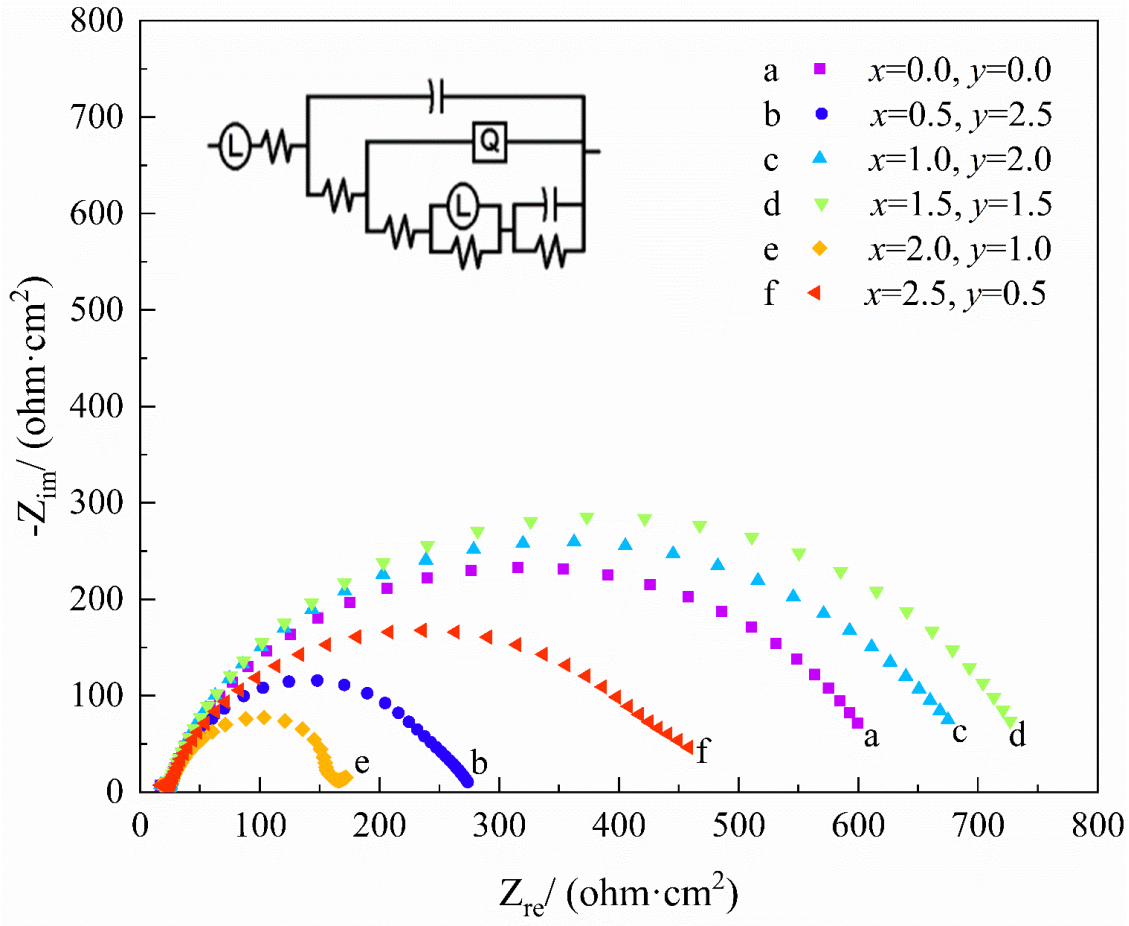

Figure 3. Nyquist plots of Mg-10Li-3Al-3Zn electrodes discharged with the existence of *x* mM Zn^{2+} and *y* mM SDBS in 0.7 M NaCl electrolyte solution.

Table 3. Polarization resistance (R_p) obtained from the Nyquist plots recorded in Figure 3.

x mM Zn^{2+} + *y* mM SDBS	$R_p/\Omega \cdot cm^2$
x=0.0, *y*=0.0	578
x=0.5, *y*=2.5	251
x=1.0, *y*=2.0	652
x=1.5, *y*=1.5	704
x=2.0, *y*=1.0	146
x=2.5, *y*=0.5	436

It is obvious that the combination of 2.0 mM Zn^{2+} and 1.0 mM SDBS minimized the impedance

of the electrode, and 432 $\Omega \cdot cm^2$ was smaller than without additives, indicating that the electrode in the mixed electrolyte solution that contained the additives had the highest discharge activity. This can be explained in that a small amount of SDBS formed a sparse and uneven film on the electrode surface, which boosted the self-corrosion rate instead of strengthening the corrosion resistance. Moreover, enough SO_4^{2-} converted neutral electrolyte solution to a weakly acidic solution, which activated the electrode and weakened the anodic polarization. Under the combined action of 2.0 mM Zn^{2+} and 1.0 mM SDBS, it is easy for oxide layers to breakdown and shed from the electrode surface, which improved the effective discharge area. As a result, charge transfer became easy, which contributed to the decline in R_p. Lv et al. [31,37] found that 0.8 mM NaF and 0.2 mM Na_2SnO_3 decreased the R_p of Mg-11Li-3.5Al-1Zn-1Sn-1Ce-0.1Mn electrodes and Mg-8Li electrodes in a 0.7 M NaCl solution from 650 $\Omega \cdot cm^2$ to 500 $\Omega \cdot cm^2$ and from 420 $\Omega \cdot cm^2$ to 340 $\Omega \cdot cm^2$, respectively. Compared to above experiments, the combination of 2.0 mM Zn^{2+} and 1.0 mM SDBS weakened R_p of Mg-Li base alloy electrodes to a greater extent because the R_p was decreased by 432 $\Omega \cdot cm^2$. Compared with NaF and Na_2SnO_3, the combination of Zn^{2+} and SDBS activated the electrodes and decreased R_p of Mg-Li base alloy electrodes more obviously. Richu Wang et al. [28] found that increasing lithium content declined R_p of Mg-3 wt.% Al alloys in a 3.5 wt.% NaCl solution from 1650 $\Omega \cdot cm^2$ to 950 $\Omega \cdot cm^2$, whose rate of decline was 42.42%. By comparison, 2.0 mM Zn^{2+} and 1.0 mM SDBS decreased R_p of Mg-10Li-3Al-3Zn alloys from 578 $\Omega \cdot cm^2$ to 146 $\Omega \cdot cm^2$, whose rate of decline was 74.74%. Although lithium is "activation" element, its ability to promote charge transfer is weaker than 2.0 mM Zn^{2+} and 1.0 mM SDBS, which illustrates that the combination of 2.0 mM Zn^{2+} and 1.0 mM SDBS has a better effect on activating magnesium alloy electrodes than lithium. Nyquist plots of AZ31 magnesium alloys in a 3.5 wt.% NaCl solution after being pretreated by phosphate solution with 0.5 g L^{-1} NaF show that 0.8 g L^{-1} Na_2MoO_4 decreased R_p of AZ31 magnesium alloys from 440 $\Omega \cdot cm^2$ to 280 $\Omega \cdot cm^2$ [38], whose rate of decline was also smaller than that of 2.0 mM Zn^{2+} and 1.0 mM SDBS. It illustrates that inorganic salt-organic salt binary additives have a better influence on activating magnesium alloy electrodes than NaF-Na_2MoO_4 additives.

In contrast, the highest impedance emerged in the mixed electrolyte solution including 1.5 mM Zn^{2+} and 1.5 mM SDBS, 126 Ω cm^2 higher than that without additives, illustrating that this concentration of additives reduced the discharge activity of electrodes. The reason for this is that the generated $Mg(OH)_2$ and $Zn(OH)_2$ were attached to the electrode surface, inhibited the shedding of the magnesium anode and hindered charge transfer. Meanwhile, with further improvements in the concentration of SDBS, multilayer protective films formed on the electrode surface to impede charge transfer. Consequently, charge transfer between the electrolyte and the magnesium anode became so difficult that R_p increased. This result corresponds to the previously mentioned potentiostatic current-time curves (Figure 2(a), 2(b) and 2(c)).

3.4. Surface morphologies of the electrode after discharging

Figures 4(a) and 4(b) respectively display SEM images of Mg-10Li-3Al-3Zn electrodes after discharging at −1.2 V for 1000 s in 0.7 mol L^{-1} NaCl solution without additives and with 2.0 mM Zn^{2+} and 1.0 mM SDBS.

In Figure 4(a), in the absence of additives, the electrode surface showed a small number of narrow

cracks with widths of approximately 20 μm, which certified that the discharge products broke down and peeled from the electrode surface with difficulty, insulating the anode surface and the electrolyte to decrease the effective discharge area. Therefore, the process of charge transfer was impeded.

By contrast, in Figure 4(b), it is shown that broader and deeper channels with widths of approximately 80 μm were distributed on the discharged anode surface evenly after discharging in the mixed electrolyte additives. These wider and deeper channels allowed the electrolyte to penetrate the inner parts of the magnesium alloys and made the oxidation products peel off more easily, which enlarged the effective discharge area. Furthermore, these channels were wider than the channels that appeared on the Mg-Li base alloy electrode after discharging in 0.7 M NaCl solution mixed with 0.20 mM Na_2SnO_3 or 0.8 mM NaF [31,37]. Yanzhuo Lv et al. [34] found that doping more zinc in Mg-Li-based alloys generated even cracks instead of deeper and larger channels on the surface of Mg-8Li-3Al-1.0Zn electrodes, which indicates that elemental zinc as an electrolyte additive with the combination of SDBS has a better influence on enlarging the effective discharge area than it as an alloy agent. Accordingly, the combination of 2.0 mM Zn^{2+} and 1.0 mM SDBS had a greater effect on enlarging the effective discharge area and promoting the electrodes to generate higher discharge current densities.

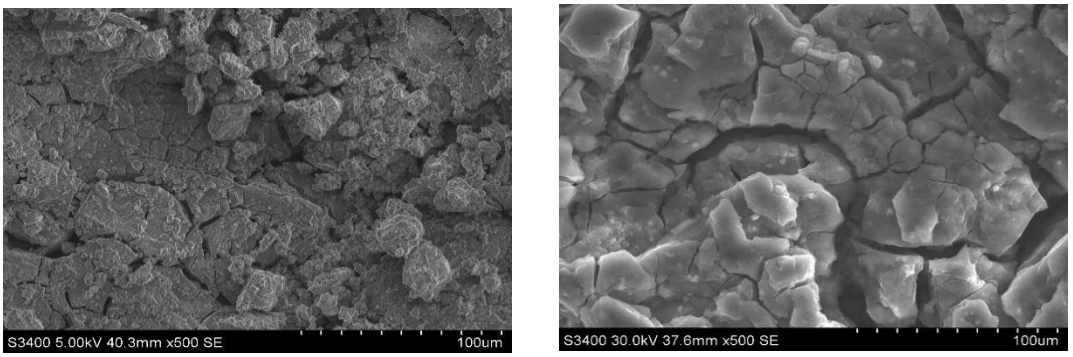

(a) (b)

Figure 4. SEM images of Mg-10Li-3Al-3Zn electrodes obtained after discharging at −1.2 V in 0.7 M NaCl solution (a) without additives and (b) with 2.0 mM Zn^{2+} and 1.0 mM SDBS for 1000s.

Figures 5(a) and 5(b) respectively exhibit EDS patterns of the discharge products achieved from the 0.7 M NaCl electrolyte solution without additives and with 2.0 mM Zn^{2+} and 1.0 mM SDBS. The contents of the elements in the discharge products are displayed in the top-right corner of the EDS patterns.

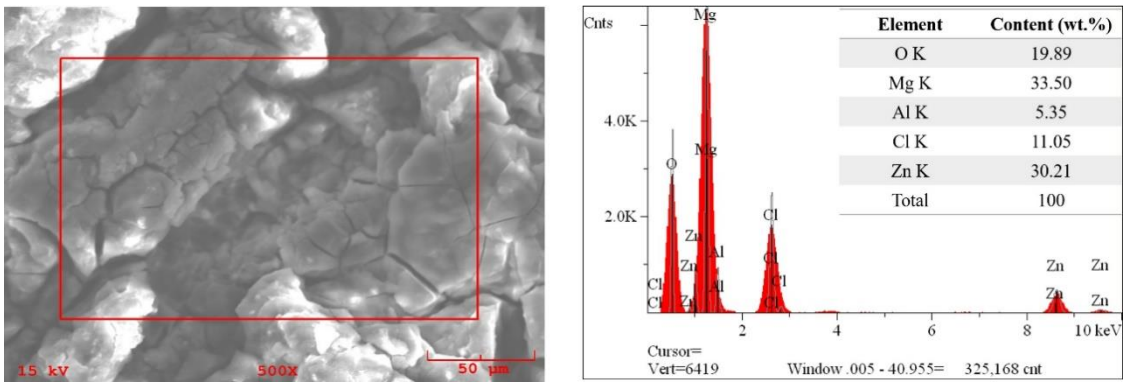

(a)

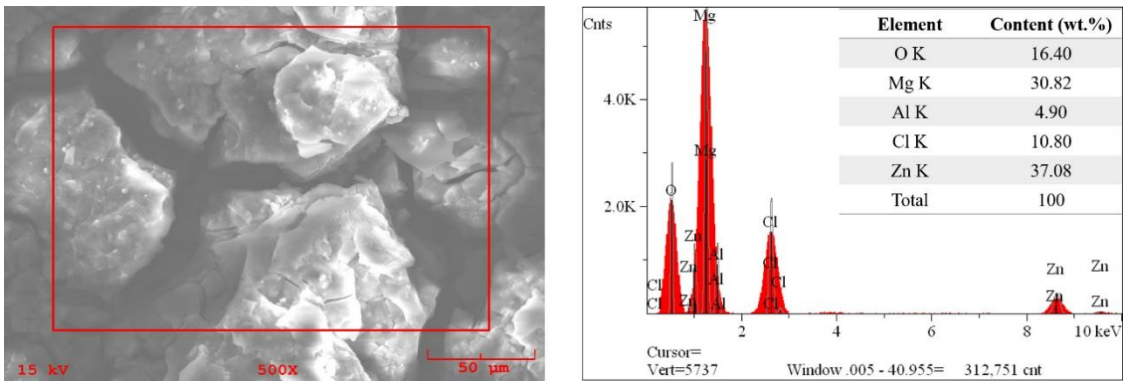

(b)

Figure 5. EDS patterns of discharge products on the Mg-10Li-3Al-3Zn electrode surface in 0.7 M NaCl solution (a) without additives and (b) with 2.0 mM Zn^{2+} and 1.0 mM SDBS.

Figure 5(a) and Figure 5(b) show that the additives obviously altered the contents of discharge products. The presence of additives decreased the content of elemental Mg from 33.50% to 30.82%, illustrating that during discharge, a large number of magnesium ions were transformed to magnesium ions in solution, which enhanced the discharge activity of electrodes. Meanwhile, additives increased the content of elemental zinc from 30.21 to 37.08%, demonstrating that more zinc ions were replaced by magnesium to attach zinc metal attaching to the electrode surface. Moreover, the decrease in the content of elemental oxygen from 19.89 to 16.40% certified that the combined action of SO_4^{2-} and SDBS facilitated the breaking of oxides from the electrode surface, which increased the effective discharge area. The results further demonstrated that Zn^{2+} and SDBS together played the roles in strengthening the discharge activation of Mg-10Li-3Al-3Zn electrodes.

The results obtained from SEM and EDS are consistent with the conclusions based on from potentiodynamic polarization curves, potentiostatic current-time curves (Figure 2(a), 2(b) and 2(c)) and Nyquist plots.

4. CONCLUSION

1. Various concentrations of Zn^{2+}-SDBS electrolyte additives have varied influence on inhibiting the corrosion of Mg-10Li-3Al-3Zn electrodes in a 0.7 M NaCl solution. With an increase in the concentration of Zn^{2+} and a decrease in the concentration of SDBS, the corrosion potential first increased and then decreased.

2. The discharge current density of Mg-10Li-3Al-3Zn electrodes in a 0.7 mol L^{-1} NaCl solution including 2.0 mM Zn^{2+} and 1.0 mM SDBS was higher than that of other concentrations of additives under constant potentials of –1.4, –1.2 and –1.0 V. By contrast, the mixture of 1.5 mM Zn^{2+} and 1.5 mM SDBS made the electrode generate the smallest discharge current density at –1.4, –1.0 and –0.8 V.

3. Additives consisting of 2.0 mM Zn^{2+} and 1.0 mM SDBS made the fractures of the oxidation products wider, deeper and more homogeneous, such that the electrolyte easily penetrated the

channels, which improved the discharge activities of the Mg-10Li-3Al-3Zn electrodes.

The electrolyte additives that contained both Zn^{2+} and SDBS significantly enhanced the electrochemical performances of Mg-10Li-3Al-3Zn electrodes in a 0.7 M NaCl electrolyte solution, which was investigated by SEM, EDS, EIS, potentiodynamic polarization tests and potentiostatic oxidation tests. The combination of 2.0 mM Zn^{2+} and 1.0 mM SDBS had the optimal influence on enhancing the discharge activity of Mg-10Li-3Al-3Zn electrodes. This study contributes to electrochemical research by filling a gap in utilizing inorganic salt-organic salt binary additives to improve the electrochemical performance of magnesium-lithium-based alloys.

ACKNOWLEDGEMENT
The authors gratefully acknowledge the financial support of the Fundamental Research Fund for the Central University (HEUCFG201842) and the National Natural Science Foundation of China (NSFC21876035).

CONFLICT OF INTEREST
The authors declare that they have no conflict of interest.

References

1. Y. Z. Lv, L. L. Bao, F. Meng and X. Gao, *Ionics*, 24 (2018) 1715.
2. L. M. Sun, L. L. Shi, S. S. Zhang, Y. J. Zhang, Z. H. Li and W. He, *J. Inorg. Mater.*, 33 (2018) 81.
3. L. Sun, L. Shi, S. Zhang, W. He and Y. Zhang, *Fuel Cells*, 17 (2017) 898.
4. 4.Y. C. Zhao, G. S. Huang, C. Zhang, C. Peng and F. S. Pan, *Int. J. Electrochem. Sci.*, 13 (2018) 8953.
5. C. S. Li, Y. Sun, F. Gebert and S. L. Chou, *Adv. Energy. Mater.*, 7 (2017) 1700869.
6. X. Li, H. Lu, S. Yuan, J. Bai, J. Wang, Y. Cao, Q. Hong, *J. Electrochem. Soc.*, 164 (2017) A3131.
7. T. Zhang, Z. Tao and J. Chen, *Mater. Horiz.*, 1 (2014) 196.
8. N. Yoshimoto, S. Yakushiji, M. Ishikawa and M. Morita, *Electrochim. Acta*, 48 (2003) 2317.
9. O. Chusid, Y. Gofer, H. Gizbar, Y. Vestfrid, E. Levi, D. Aurbach and I. Riech, *Adv. Mater.*, 15 (2003) 627.
10. X. W. Miao, J. Yang, W. J. Pan, H. C. Yuan, Y. N. Nuli and S. Hirano, *Electrochim. Acta*, 210 (2016) 704.
11. S. Tao, W. F. Huang, Y. S. Liu, S. M. Chen, B. Qian and L. Song, *J. Mater. Chem. A*, 6 (2018) 8210.
12. Y. H. Tan, W. T. Yao, T. W. Zhang, T. Ma, L. L. Liu, F. Zhou, H. B. Yao and S. H. Yu, *ACS Nano*, 12 (2018) 5856.
13. K. Mahesh, R. Balaji and K. S. Dhathathreyan, *Ionics*, 21 (2015) 2603.
14. C. Shu, E. Wang, L. Jiang, Q. Tang and G. Sun, *J. Power Sources*, 208 (2012) 159.
15. Y. Z. Lv, Y. Z. Jin, Z. B. Wang, M. Liu, Y. F. Li, L. Wang and D. X. Cao, *Ionics*, 21 (2015) 429.
16. K. Mahesh, R. Balaji and K. S. Dhathathreyan, *Ionics*, 21 (2015) 2603.
17. N. Wang, R. Wang, C. Peng, Y. Feng, *Corros. Sci.*, 81 (2014) 85.
18. L. J. Liu and M. Schlesinger, *Corros. Sci.*, 51 (2009) 1733.
19. L. Wen, K. Yu, H. Xiong, Y. Dai, S. Yang, X. Qiao, F. Teng, S. Fan, *Electrochim. Acta*, 194 (2016) 40.
20. Y. Feng, R. Wang, K. Yu, C. Peng, J. Zhang and C. Zhang, *J. Alloys Compd.*, 473 (2009) 215.
21. Y. P. Wu, Z. F. Wang, Y. Liu, G. F. Li, S. H. Xie, H. Yu, H. Q. Xiong, *Int. J. Electrochem. Sci.*, 13

(2018) 10325.
22. M. Yuasa, X. Huang, K. Suzuki and M. Mabuchi, *J. Power Sources*, 297 (2015) 449.
23. L. L. Shi, Y. J. Xu, K. Li, Z. P. Yao and S. Q. Wu, *Curr. Appl. Phys.*, 10 (2010) 719.
24. Q. F. Li and N. J. Bjerrum, *J. Power Sources*, 110 (2002) 1.
25. Y. D. Yan, D. B. Ji, Y. Xue, M. L. Zhang, P. Wang, Y. H. Liu, T. Q. Yin, P. Li, W. Han and J. Wang, *J. Electrochem. Soc.*, 164 (2017) D429.
26. D. B. Ji, T. Q. Yin, Y. D. Yan, M. L. Zhang, P. Wang, Y. H. Liu, J. N. Zheng, Y. Xue, X. Y. Jing and W. Han, *RSC Adv.*, 6 (2016) 29353.
27. R. C. Zeng, L. Sun, Y. F. Zheng, H. Z. Cui and E. H. Han, *Corros. Sci.*, 79 (2014) 69.
28. R. C. Wang, Q. Li, N. G. Wang, C. Q. Peng and Y. Feng, *J Mater. Eng. Perform.*, 21 (2018) 6552.
29. A. Sivashanmugam, T. P. Kumar, N. G. Renganathan and S. Gopukumar, *J. Appl. Electrochem.*, 34 (2004) 1135.
30. N. G. Wang, R. C. Wang, Y. Feng, W. H. Xiong, J. C. Zhang and M. Deng, *Corros. Sci.*, (2016), http://dx.doi.org/10.1016/j.corsci.2016.07.002
31. Y. Z. Lv, L. Wang, Y. F. Li, Y. Z. Jin, J. Feng, Y. M. Ren, D. X. Cao, G. L. Wang and M. L. Zhang, *Ionics*, 20 (2014) 1573.
32. D. X. Cao, L. Wu, Y. Sun, G. L. Wang and Y. Z. Lv, *J. Power Sources*, 177 (2008) 624.
33. W. W. Zheng, The pilot study of electrochemical characteristics of magnesium in different electrolyte solution, Master Thesis, Tianjin, China, 2009, 34.
34. Y. Z. Lv, M. Liu, Y. Xu, D. X. Cao and J. Feng, *J. Power Sources*, 225 (2013) 124.
35. V. Pavlyuk, D. Kulawik, W. Ciesielski, N. Pavlyuk and G. Dmytriv, *Acta Cryst.*, C74 (2018) 360.
36. M. Anik and G. Celikten, *Corros. Sci.*, 49 (2007) 1878.
37. Y. Z. Lv, D. D. Tang, D. X. Cao, G. L. Wang, M. L. Zhang and J. Feng, *RSC Adv.*, 5 (2015) 46423.
38. T. T. Wan, Z. X. Liu, M. Z. Bu and P. C. Wang, *Corros. Sci.*, 66 (2013) 33.